ISR e^+e^- to charm at Belle

G.Pakhlova
ITEP, Moscow, Russia

Introduction

Studies of exclusive open charm production near threshold in e^+e^- annihilation provide important information on the dynamics of charm quarks and on the properties of the ψ states.

Another motivation for studying exclusive open charm production is the existence of charmonium-like states with masses above open-charm threshold and quantum numbers $J^{PC} = 1^{--}$. Although these have been known for over four years, the nature of these states, found in $e^+e^- \to \pi^+\pi^- J/\psi(\psi(2S))\gamma_{\rm ISR}$ processes, remains unclear. Among them are the $Y(4260)$ state observed by BaBar [1, 2], confirmed by CLEO [3, 4] and Belle [5]; the $Y(4350)$ discovered by BaBar [6] and confirmed by Belle [7]; two structures, the $Y(4008)$ and the $Y(4660)$ seen by Belle [5, 7].

The absence of open charm decay channels for Y states, large partial widths for decay channels to charmonium plus light hadrons and the lack of available $J^{PC} = 1^{--}$ charmonium levels are inconsistent with the interpretation of the Y states as conventional charmonia. To explain the observed peaks, some models assign the $3^3D_1(4350)$, $5^3S_1(4660)$ with shifted masses [8], other explore coupled-channel effects and rescattering of charm mesons [9]. More exotic suggestions include hadro-charmonium [10]; multiquark states, such as a $[cq][\overline{cq}]$ tetraquark [11] and $D\overline{D}_1$ or $D^0\overline{D}^{*0}$ molecules [12]. One of the most popular exotic options for the Y states are the hybrids expected by LQCD in the mass range from $4.2-5.0\,{\rm GeV}/c^2$ [13]. In this context, some authors expect the dominant decay channels of the Y(4260) to be $Y(4260) \to D^{(*)}\overline{D}^{(*)}\pi$.

During the past three years numerous measurements of exclusive e^+e^- cross sections for charmed hadron pairs have been reported. Most of these measurements were performed at B-factories using initial-state radiation (ISR). Here we present Belle results on the e^+e^- cross sections to the $D\overline{D}$, D^+D^{*-} [14], $D^{*+}D^{*-}$, $D^0D^-\pi^+$ [15, 16, 17], $\Lambda_c^+\Lambda_c^-$ [18] and $D^0D^{*-}\pi^+$ final states [19]. The data sample corresponds to a large integrated luminosity collected with the Belle detector [20] at the $\Upsilon(4S)$ resonance and nearby continuum at the KEKB asymmetric-energy e^+e^- collider [21].

Measurement of the near-threshold $e^+e^- \to D^{(*)\pm}D^{*\mp}$ cross section

To select $e^+e^- \to D^{(*)+}D^{*-}\gamma_{\rm ISR}$ signal events we use a method that achieves high efficiency by requiring full reconstruction of only one of the $D^{(*)+}$ mesons, the $\gamma_{\rm ISR}$, and the slow $\pi^-_{\rm slow}$ from the other D^{*-}. In this case the spectrum of masses recoiling against the $D^{(*)+}\gamma_{\rm ISR}$ system:

$$M_{\rm rec}(D^{(*)+}\gamma_{\rm ISR}) = \sqrt{(E_{\rm c.m.} - E_{D^{(*)+}\gamma_{\rm ISR}})^2 - p^2_{D^{(*)+}\gamma_{\rm ISR}}} \quad (1)$$

peaks at the D^{*-} mass. Here $E_{D^{(*)+}\gamma_{\rm ISR}}$ and $p_{D^{(*)+}\gamma_{\rm ISR}}$ are the c.m. energy and momentum, respectively, of the $D^{(*)+}\gamma_{\rm ISR}$ combination. This peak is expected to be wide and asymmetric due to the photon energy resolution and higher-order corrections to ISR. The resolution of this peak (estimated to be $\sim 300\,{\rm MeV}/c^2$) is not sufficient to separate the $D\overline{D}^*$, $D^*\overline{D}^*$ or $D^{(*)}\overline{D}^*\pi$ final states. To disentangle the contributions from these final states and to suppress combinatorial backgrounds, we use the slow pion from the unreconstructed D^{*-}. The difference between the mass recoiling against $D^{(*)+}\gamma_{\rm ISR}$ and $D^{(*)+}\pi^-_{\rm slow}\gamma_{\rm ISR}$ (recoil mass difference):

$$\Delta M_{\rm rec} = M_{\rm rec}(D^{(*)+}\gamma_{\rm ISR}) - M_{\rm rec}(D^{(*)+}\pi^-_{\rm slow}\gamma_{\rm ISR})\,, \quad (2)$$

has a narrow distribution ($\sigma \sim 1.4\,{\rm MeV}/c^2$) around the $m_{D^{*-}} - m_{\overline{D}^0}$, since the uncertainty in $\gamma_{\rm ISR}$ momentum partially cancels out.

For the measurement of the exclusive cross section we determine the $D^{(*)+}D^{*-}$ mass ($\equiv M_{\rm rec}(\gamma_{\rm ISR})$ in the absence of higher-order QED processes). The photon energy resolution results in a typical $M_{\rm rec}(\gamma_{\rm ISR})$ resolution of $\sim 100\,{\rm MeV}$, which is too big for a study of relatively narrow $D^{(*)+}D^{*-}$ mass states. We significantly improve the $M_{\rm rec}(\gamma_{\rm ISR})$ resolution by applying a refit that constrains $M_{\rm rec}(D^{(*)+}\gamma_{\rm ISR})$ to the D^{*-} mass. As a result, the $M_{D^{(*)+}D^{*-}}$ resolution is improved by a factor of ~ 10. The recoil mass difference after the refit procedure ($\Delta M^{\rm fit}_{\rm rec}$) has a resolution improved by a factor of ~ 2. We define the signal region by the requirement that $M_{\rm rec}(D^{*+}\gamma_{\rm ISR})$ be within $\pm 0.2\,{\rm GeV}/c^2$ of the D^{*-} mass and by the tight requirement on $\Delta M^{\rm fit}_{\rm rec}$ within $\pm 2\,{\rm MeV}/c^2$ of the $m_{D^{*-}} - m_{\overline{D}^0}$.

The $e^+e^- \to D^{(*)+}D^{*-}$ cross sections are extracted from the $D^{(*)+}D^{*-}$ mass distributions after background subtraction by the relation described in [16]. The resulting exclusive $e^+e^- \to D^{(*)+}D^{*-}$ cross sections are shown in Fig. 1 with statistical uncertainties only. The total systematic uncertainties are (11)10% and comparable to the statistical errors in the differential cross section.

The shape of the $e^+e^- \to D^{*+}D^{*-}$ cross section is complicated with several local maxima and minima. Aside from a prominent excess near threshold, the $e^+e^- \to D^+D^{*-}$ cross section is relatively featureless. The measured cross sections are compatible [22] within errors with the $D^{(*)}\overline{D}^*$ exclusive cross section measured by BaBar [23] and CLEO-c [24].

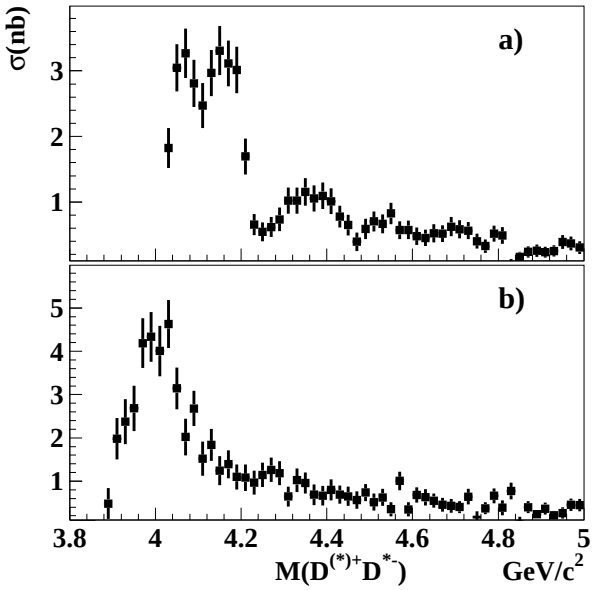

Figure 1: The exclusive cross sections for (a) $e^+e^- \to D^{*+}D^{*-}$ and (b) $e^+e^- \to D^+D^{*-}$.

Measurement of the near-threshold $e^+e^- \to D\overline{D}$ cross section

We select $e^+e^- \to D\overline{D}\gamma_{\rm ISR}$ signal events by reconstructing both the D and $\overline{D}$ mesons, where $D = D^0$ or D^+. In general, the $\gamma_{\rm ISR}$ is not required to be detected; its presence in the event is inferred from a peak at zero in the spectrum of the recoil mass against the $D\overline{D}$ system. The square of the recoil mass is defined as:

$$M^2_{\rm rec}(D\overline{D}) = (E_{\rm c.m.} - E_{D\overline{D}})^2 - p^2_{D\overline{D}}, \qquad (3)$$

where $E_{D\overline{D}}$ and $p_{D\overline{D}}$ are the c.m. energy and momentum of the $D\overline{D}$ combination, respectively. To suppress backgrounds we consider two cases: (1) the $\gamma_{\rm ISR}$ is out of detector acceptance in which case the polar angle for the $D\overline{D}$ combination in the c.m. frame is required to be $|\cos(\theta_{D\overline{D}})| > 0.9$; (2) the fast $\gamma_{\rm ISR}$ is within the detector acceptance ($|\cos(\theta_{D\overline{D}})| < 0.9$), in this case the $\gamma_{\rm ISR}$ is required to be detected and the mass of the $D\overline{D}\gamma_{\rm ISR}$ combination is required to be greater than $E_{\rm c.m.} - 0.58\,{\rm GeV}/c^2$. To suppress background from $e^+e^- \to D\overline{D}(n)\pi\gamma_{\rm ISR}$ processes we exclude events that contain additional charged tracks that are not used in the D or $\overline{D}$ reconstruction. To suppress the tail of $e^+e^- \to D^{(*)}\overline{D}^{(*)}(n)\pi^0\gamma_{\rm ISR}$ events we define a signal region by the requirement: $|M^2_{\rm rec}(D\overline{D})| < 0.7({\rm GeV}/c^2)^2$.

The resulting $e^+e^- \to D^0\overline{D}^0$, $e^+e^- \to D^+D^-$ and $e^+e^- \to D\overline{D}$ exclusive cross sections, averaged over the bin width, are shown in Fig. 2 with statistical uncertainties only. The total systematic uncertainties are 10% and comparable to the statistical errors in the differential cross section around the $\psi(3770)$ peak; for the other $M_{D\overline{D}}$ ranges statistical errors dominate. The observed $e^+e^- \to D\overline{D}$ exclusive cross sections are consistent with BaBar measurements [25]. This includes a peak at $3.9\,{\rm GeV}/c^2$ that is seen both in Belle and BaBar mass spectra.

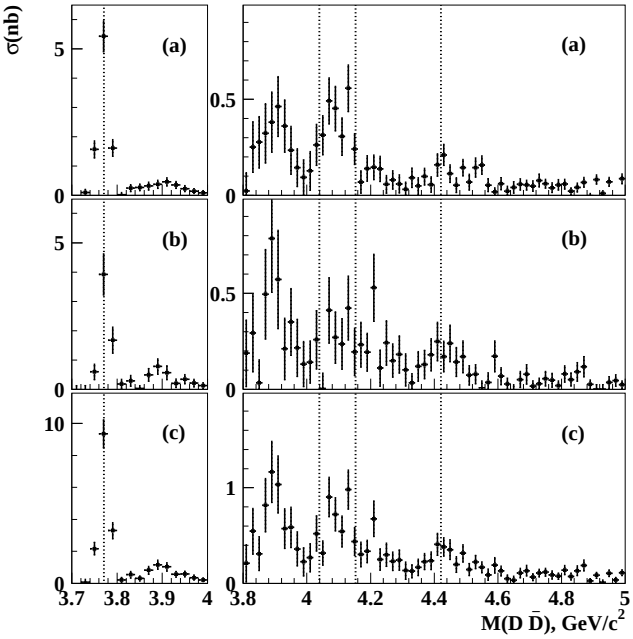

Figure 2: The exclusive cross sections for: (a) $e^+e^- \to D^0\overline{D}^0$; (b) $e^+e^- \to D^+D^-$; (c) $e^+e^- \to D\overline{D}$. The dotted lines correspond to the $\psi(3770)$, $\psi(4040)$, $\psi(4160)$ and $\psi(4415)$ masses.

We calculate the cross section ratio $\sigma(e^+e^- \to D^+D^-)/\sigma(e^+e^- \to D^0\overline{D}^0)$ for the $M_{D\overline{D}}$ bin $(3.76-3.78)\,{\rm GeV}/c^2$ corresponding to $M_{D\overline{D}} \approx M_{\psi(3770)}$ to be $(0.72 \pm 0.16 \pm 0.06)$. This value is in agreement within errors with CLEO-c [26] and BES [27] measurements. The ratio $\sigma(e^+e^- \to D^+D^-)/\sigma(e^+e^- \to D^0\overline{D}^0)$ integrated over the $M_{D\overline{D}}$ range from 3.8 to 5.0 ${\rm GeV}/c^2$ is found to be $(1.15 \pm 0.13 \pm 0.10)$ and is consistent with unity.

Observation of $\psi(4415) \to D\overline{D}^*_2(2460)$ decay

We use the similar full reconstruction method described above to select $e^+e^- \to D^0D^-\pi^+\gamma_{\rm ISR}$ signal candidates. The $e^+e^- \to D^0D^-\pi^+$ cross section extracted from the background-subtracted $D^0D^-\pi^+$ mass distribution is shown in Fig. 3.

To study the resonant structure in $\psi(4415)$ decays, we select $D^0D^-\pi^+$ combinations from a $\pm 100\,{\rm MeV}/c^2$ mass window around the $\psi(4415)$ mass [28]. A scatter plot of $M(D^-\pi^+)$ vs. $M(D^0\pi^+)$ and its projections onto both axes evidently demonstrate clear signals for the $\overline{D}^*_2(2460)^0$ and $D^*_2(2460)^+$ mesons and positive interference between the neutral $D^0\overline{D}^*_2(2460)^0$ and the charged $D^-D^*_2(2460)^+$ decay amplitudes leading to the same $D^0D^-\pi^+$ final state for the decay of $C = -1$ state. Because of the interference we do not study $D^0\overline{D}^*_2(2460)^0$ and $D^-D^*_2(2460)^+$

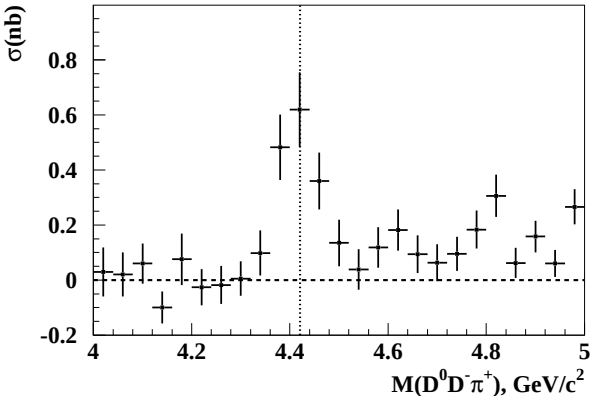

Figure 3: The exclusive cross section for $e^+e^- \to D^0D^-\pi^+$. The dotted line corresponds to the mass of the $\psi(4415)$.

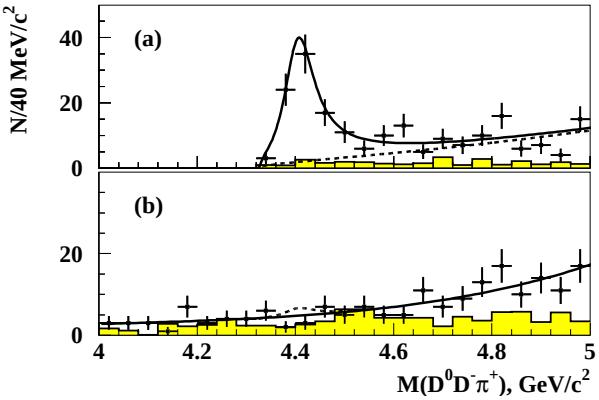

Figure 4: (a) The $M_{D^0D^-\pi^+}$ spectrum for the $D\overline{D}{}^*_2(2460)$ signal region. The threshold function is shown by the dashed curve. (b) The $M_{D^0D^-\pi^+}$ spectrum outside the $D\overline{D}{}^*_2(2460)$ signal region. The dashed curve shows the upper limit on the $\psi(4415)$ yield at 90% C.L. Histograms show the normalized contributions from M_{D^0} and M_{D^-} sidebands.

final states separately and define the signal interval for the $D\overline{D}{}^*_2(2460)$ combinations as $|M_{D^-\pi^+} - m_{\overline{D}{}^*_2(2460)^0}| < 50\,\mathrm{MeV}/c^2$ or $|M_{D^0\pi^+} - m_{D^*_2(2460)^+}| < 50\,\mathrm{MeV}/c^2$.

We perform a separate study of $e^+e^- \to D\overline{D}{}^*_2(2460)$ and $e^+e^- \to D(\overline{D}\pi)_{\mathrm{non}\overline{D}{}^*_2(2460)}$. The $M_{D^0D^-\pi^+}$ spectrum for the $D\overline{D}{}^*_2(2460)$ signal interval is shown in Fig. 4(a). A clear peak corresponding to $\psi(4415) \to D\overline{D}{}^*_2(2460)$ decay is evident near the $D\overline{D}{}^*_2(2460)$ threshold. To compare mass and width of the obtained $\psi(4415)$ signal with the corresponding $\psi(4415)$ resonance parameters measured in the *inclusive* study, we perform a likelihood fit to $M_{D^0D^-\pi^+}$ distribution with the $D\overline{D}{}^*_2(2460)$ signal parameterized by an s-wave RBW function. To account for background and a possible non-resonant $D^0D^-\pi^+$ contribution we use a threshold function $\sqrt{M - m_D - m_{\overline{D}{}^*_2(2460)}}$ with a floating normalization. Finally, the sum of the signal and background functions is multiplied by the mass-dependent linear efficiency function and differential ISR luminosity. The fit, shown as a solid curve in Fig. 4(a), yields $109 \pm 25(\mathrm{stat.})$ signal events. The significance for the signal is obtained to be $\sim 10\sigma$. The obtained peak mass $m_{\psi(4415)} = (4.411 \pm 0.007(\mathrm{stat.}))\,\mathrm{GeV}/c^2$ and total width $\Gamma_{\mathrm{tot}} = (77 \pm 20(\mathrm{stat.}))\,\mathrm{MeV}/c^2$ are in good agreement with the PDG [28] values and the BES results [29]. The peak cross section for $e^+e^- \to \psi(4415) \to D\overline{D}{}^*_2(2460)$ process at $E_{\mathrm{c.m.}} = m_{\psi(4415)}$ is calculated from the amplitude of the RBW function in the fit to be $\sigma(e^+e^- \to \psi(4415)) \times \mathcal{B}(\psi(4415) \to D\overline{D}{}^*_2(2460)) \times \mathcal{B}(\overline{D}{}^*_2(2460) \to D\pi^+) = (0.74 \pm 0.17 \pm 0.08)\,\mathrm{nb}$. Using $\sigma(e^+e^- \to \psi(4415)) = 12\pi/m^2_{\psi(4415)} \times (\Gamma_{ee}/\Gamma_{\mathrm{tot}})$ we calculate the $\mathcal{B}(\psi(4415) \to D\overline{D}{}^*_2(2460)) \times \mathcal{B}(\overline{D}{}^*_2(2460) \to D\pi^+) = (10.5 \pm 2.4 \pm 3.8)\%$ using the $\psi(4415)$ parameters from the PDG [28] and $(19.5 \pm 4.5 \pm 9.2)\%$ for the $\psi(4415)$ parameters from Ref. [29].

The shape of the $M_{D^0D^-\pi^+}$ spectrum with the $D\overline{D}{}^*_2(2460)$ signal excluded, shown as a solid curve in Fig. 4(b), in the $\psi(4415)$ mass window, is consistent with the combinatorial background. We obtain $\mathcal{B}(\psi(4415) \to D^0D^-\pi^+_{\mathrm{non-resonant}})/\mathcal{B}(\psi(4415) \to D\overline{D}{}^*_2(2460) \to D^0D^-\pi^+) < 0.22$ at 90% C.L.

Measurement of the near-threshold $e^+e^- \to \Lambda_c^+\Lambda_c^-$ cross section

The selection of $e^+e^- \to \Lambda_c^+\Lambda_c^-\gamma_{\mathrm{ISR}}$ signal events using full reconstruction of both the Λ_c^+ and Λ_c^- baryons suffers from the low Λ_c reconstruction efficiency and small branching fractions for decays to accessible final states. Therefore, in order to achieve higher efficiency we require full reconstruction of only one of the Λ_c baryons and the γ_{ISR} photon. In this case the spectrum of masses recoiling against the $\Lambda_c^+\gamma_{\mathrm{ISR}}$ system peaks at the Λ_c^- mass.

For the measurement of the exclusive cross section for $e^+e^- \to \Lambda_c^+\Lambda_c^-$, we determine the mass recoiling against the γ_{ISR} photon ($M_{\mathrm{rec}}(\gamma_{\mathrm{ISR}})$). To improve the $M_{\mathrm{rec}}(\gamma_{\mathrm{ISR}})$ resolution (expected to be $\sim 100\,\mathrm{MeV}/c^2$), we apply a refit that constrains $M_{\mathrm{rec}}(\Lambda_c^+\gamma_{\mathrm{ISR}})$ to the nominal Λ_c^- mass. As a result, the $M_{\Lambda_c^+\Lambda_c^-}$ resolution is improved substantially; it varies from $\sim 3\,\mathrm{MeV}/c^2$ just above threshold to $\sim 8\,\mathrm{MeV}/c^2$ at $M_{\Lambda_c^+\Lambda_c^-} \sim 5.4\,\mathrm{GeV}/c^2$.

To suppress combinatorial background, we require the presence of at least one $\overline{p}$ in the event from the decay of the unreconstructed Λ_c^- ($\overline{p}$ tag). As a result, the combinatorial background is suppressed by a factor of ~ 10 at the expense of about a 40% reduction in signal.

The $M_{\Lambda_c^+\Lambda_c^-}$ spectrum for events in the signal region is shown in Fig. 5(a). A clear peak is evident near the $\Lambda_c^+\Lambda_c^-$ threshold. Assuming the observed peak to be a resonance, we perform a simultaneous likelihood fit to the $M_{\Lambda_c^+\Lambda_c^-}$ distributions for the Λ_c^+ signal and sideband regions to fix the combinatorial background shapes. As the

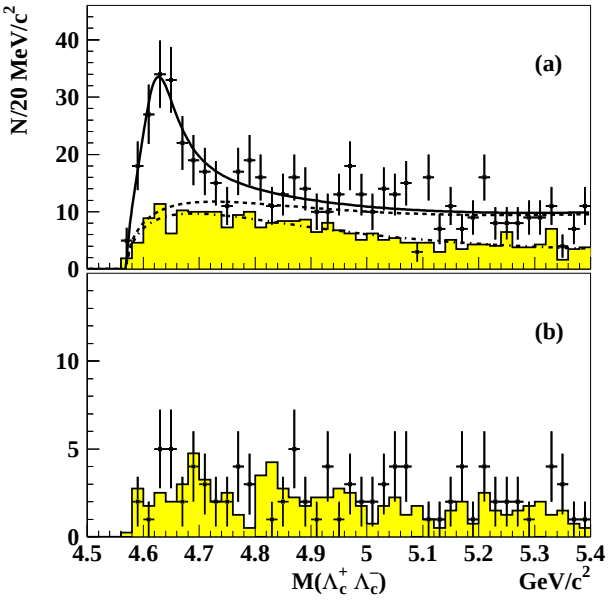

Figure 5: The $M_{\Lambda_c^+\Lambda_c^-}$ spectrum for the signal region: (a) with $\overline{p}$ tag. The solid curve represents the result of the fit described in the text. The threshold function is shown by the dashed curve. The combinatorial background parameterization is shown by the dashed-dotted curve; (b) with proton (wrong-sign) tag. Histograms show the normalized contributions from Λ_c^+ sidebands.

signal function we use a sum of a relativistic *s*-wave Breit-Wigner function and a threshold function with a floating normalization to take into account a possible non-resonant contribution. The fit, shown as a solid curve in Fig. 5 (a), attributes $142^{+32}_{-28}(\mathrm{stat.})$ events to the RBW signal. The obtained peak mass is $M = (4634^{+8+5}_{-7-8})\,\mathrm{MeV}/c^2$ and the total width is $\Gamma_{\rm tot} = (92^{+40+10}_{-24-21})\,\mathrm{MeV}$. The significance including systematics is 8.2σ. We use X(4630) to denote the observed structure.

As a cross check, we present in Fig. 5 (b) the $M_{\Lambda_c^+\Lambda_c^-}$ spectrum for the signal region for wrong-sign tags, *i.e.* requiring a presence of a proton in the event in addition to the $\Lambda_c^+\gamma_{\rm ISR}$ combination. The $M_{\Lambda_c^+\Lambda_c^-}$ distribution from the signal Λ_c^+ window is in good agreement with the normalized contributions from the Λ_c^+ sidebands.

The $e^+e^- \to \Lambda_c^+\Lambda_c^-$ cross section extracted from the background-subtracted $\Lambda_c^+\Lambda_c^-$ mass distribution is shown in Fig. 6 with statistical uncertainties only. The peak cross section for the $e^+e^- \to \Lambda_c^+\Lambda_c^-$ process at $E_{\rm c.m.} = m_{X(4630)}$ is calculated from the amplitude of the RBW function in the fit to be $\sigma(e^+e^- \to X(4630)) \times \mathcal{B}(X(4630) \to \Lambda_c^+\Lambda_c^-) = (0.47^{+0.11+0.05}_{-0.10-0.08} \pm 0.19)$ nb. We calculate $\Gamma_{ee}/\Gamma_{\rm tot} \times \mathcal{B}(X(4630) \to \Lambda_c^+\Lambda_c^-) = (0.68^{+0.16+0.07}_{-0.15-0.11} \pm 0.28) \cdot 10^{-6}$.

The nature of significant near-threshold enhancement remains unclear. In many processes including three-body B meson baryon decays, mass peaks are observed near threshold [32]. However, the cross section for $e^+e^- \to \Lambda\overline{\Lambda}$

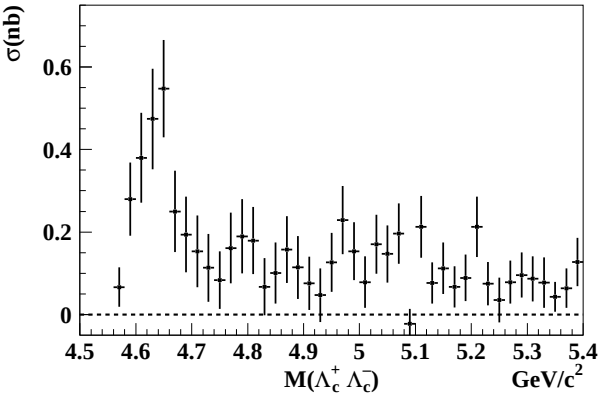

Figure 6: The cross section for the exclusive process $e^+e^- \to \Lambda_c^+\Lambda_c^-$.

measured via ISR by BaBar [30] has a different pattern: it increases sharply at threshold and then decreases gradually without any peak-like structure. Although both mass and width of the $X(4630)$ are consistent within errors with those of the $Y(4660)$, this coincidence does not exclude other interpretations of the $X(4630)$, for example, as the conventional charmonium state [31, 8] or as a baryon-antibaryon threshold effect [32].

Measurement of the near-threshold $e^+e^- \to D^0D^{*-}\pi^+$ cross section

For measurement of the $e^+e^- \to D^0D^{*-}\pi^+$ cross section we employ the reconstruction method that was used for $e^+e^- \to D\overline{D}$ and $e^+e^- \to D^0D^-\pi^+$. The resulting $e^+e^- \to D^0D^{*-}\pi^+$ exclusive cross section averaged over the bin width is shown in Fig. 7 with statistical uncertainties only. The total systematic uncertainty is 10%.

To obtain limit on $e^+e^- \to \psi(4415) \to D^0D^{*-}\pi^+$ process we perform a likelihood fit to the $M_{D^0D^{*-}\pi^+}$ distribution where we parameterize a possible $\psi(4415)$ signal contribution by an s-wave RBW function with a free normalization. We use PDG values [28] to fix its mass and total width. To take a non-resonant $D^0D^{*-}\pi^+$ contribution into account we use a threshold function $\sqrt{M - m_{D^0} - m_{D^{*-}} - m_{\pi^+}}$ with a free normalization. Finally, the sum of the signal and non-resonant functions is multiplied by a mass-dependent second-order polynomial efficiency function and differential ISR luminosity.

The fit yields $14.4 \pm 6.2^{+1.0}_{-9.5}$ signal events for the $\psi(4415)$ state. The statistical significance for the $\psi(4415)$ signal is determined to be 3.1σ. We calculate an upper limit on the peak cross section for the $e^+e^- \to \psi(4415) \to D^0D^{*-}\pi^+$ process at $E_{\rm c.m.} = m_{\psi(4415)}$ from the amplitude of the RBW function in the fit to be $\sigma(e^+e^- \to \psi(4415)) \times \mathcal{B}(\psi(4415) \to D^0D^{*-}\pi^+) < 0.76$ nb at the 90% C.L. Using $\sigma(e^+e^- \to \psi(4415)) = 12\pi/m^2_{\psi(4415)} \times (\mathcal{B}_{\rm ee})$ and PDG values of the $\psi(4415)$ mass, full width and electron width [28] we found $\mathcal{B}_{\rm ee} \times \mathcal{B}(\psi(4415) \to D^0D^{*-}\pi^+) < 0.99 \times 10^{-6}$ at the 90%

C.L and $\mathcal{B}(\psi(4415) \to D^0 D^{*-}\pi^+) < 10.6\%$ at the 90% C.L. All presented upper limit values include systematic uncertainties. For illustration we include the corresponding fit function on the cross section distribution plot shown in Fig. 7.

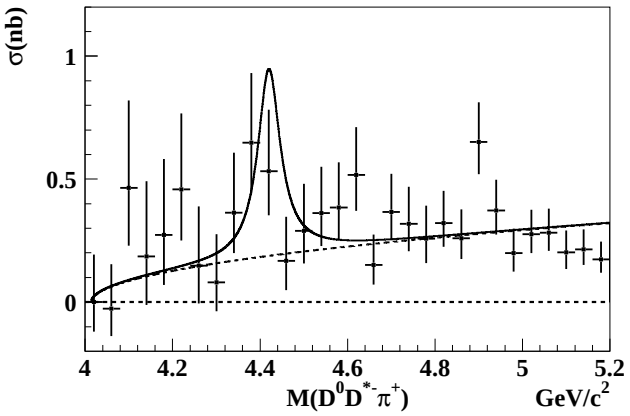

Figure 7: The exclusive cross section for $e^+e^- \to D^0 D^{*-}\pi^+$ averaged over the bin width with statistical uncertainties only. The fit function corresponds to the upper limit on $\psi(4415)$ taking into account systematic uncertainties. The solid line represents the sum of the signal and threshold contributions. The threshold function is shown by the dashed line.

To obtain limits on the decays $X \to D^0 D^{*-}\pi^+$, where X denotes $Y(4260)$, $Y(4350)$, $Y(4660)$ or $X(4630)$ states, we perform four likelihood fits to the $M_{D^0 D^{*-}\pi^+}$ spectrum each with one of the X states, the $\psi(4415)$ state and a non-resonant contribution. For fit functions we use the sum of two s-wave relativistic RBW functions with a free normalization and a threshold function $\sqrt{M - m_{D^0} - m_{D^{*-}} - m_{\pi^+}}$ with a free normalization. For masses and total widths of the $Y(4260)$ and $\psi(4415)$ states we use PDG values [28]. The corresponding parameters of the $Y(4660)$, $Y(4350)$ and $X(4630)$ states are fixed from Ref. [33, 18], respectively.

The significances for the $Y(4260)$, $Y(4350)$, $Y(4660)$ and $X(4630)$ signal are found to be 0.9σ, 1.4σ, 0.1σ and 1.8σ, respectively. The calculated upper limits (at the 90% C.L.) on the peak cross sections for $e^+e^- \to X \to D^0 D^{*-}\pi^+$ processes at $E_{\rm c.m.} = m_X$ are presented in Table 1. Using fixed values of X masses and full widths we obtain upper limits on the $\mathcal{B}_{\rm ee} \times \mathcal{B}(X \to D^0 D^{*-}\pi^+)$ at the 90% C.L. Finally, for the $Y(4260)$ state we estimate the upper limit on $\mathcal{B}(Y(4260) \to D^0 D^{*-}\pi^+)/\mathcal{B}(Y(4260) \to \pi^+\pi^- J/\psi)$ at the 90% C.L. using $\mathcal{B}_{\rm ee} \times \Gamma(\pi^+\pi^- J/\psi)$ [28]. For the $Y(4350)$ and $Y(4660)$ states we calculate $\mathcal{B}(X \to D^0 D^{*-}\pi^+)/\mathcal{B}(X \to \pi^+\pi^-\psi(2S))$ at the 90% C.L. taking into account $\mathcal{B}_{\rm ee} \times \Gamma(\pi^+\pi^-\psi(2S))$ [33]. All upper limits presented in Table 1 include systematic uncertainties.

To estimate the effects of possible interference between final states we also performed a fit to the $M_{D^0 D^{*-}\pi^+}$ spectrum that includes complete interference between the $\psi(4415)$ RBW amplitude and a non-resonant $D^0 D^{*-}\pi^+$ contribution. We found two solutions with similar goodness-of-fit; the interference is constructive for one solution and destructive for the other. From the fit with destructive interference we find an upper limit on the peak cross section for $e^+e^- \to \psi(4415) \to D^0 D^{*-}\pi^+$ process to be $\sigma(e^+e^- \to \psi(4415)) \times \mathcal{B}(\psi(4415) \to D^0 D^{*-}\pi^+) < 1.93$ nb at the 90% C.L.

In addition we performed four likelihood fits to the $M_{D^0 D^{*-}\pi^+}$ spectrum with complete interference between the X and $\psi(4415)$ states' RBW amplitudes and a non-resonant $D^0 D^{*-}\pi^+$ contribution. We found four solutions for each fit with similar goodness-of-fit and obtained the upper limits on the peak cross sections for $e^+e^- \to X \to D^0 D^{*-}\pi^+$ process to be $\sigma(e^+e^- \to X) \times \mathcal{B}(X \to D^0 D^{*-}\pi^+)$ less than 1.44, 1.92, 1.38 and 0.98 nb at the 90% C.L. for $Y(4260)$, $Y(4350)$, $Y(4660)$ and $X(4630)$, respectively.

Conclusion

The measured six open charm final states nearly saturate the total cross section for charm hadron production in e^+e^- annihilation in the $\sqrt{s}$ region up to $\sim 5\,\mathrm{GeV}$. The exclusive cross sections for charm strange meson pairs have been measured to be an order of magnitude smaller than charm meson production [24]. Charm baryon-antibaryon pair production occurs at energies above $4.5\,\mathrm{GeV}$.

Belle and BaBar found no evidence for open charm production with any of $Y(4260)$, $Y(4350)$, $Y(4660)$ and $X(4630)$ states, in particular for $Y(4260) \to D^0 D^{*-}\pi^+$ decays as predicted by hybrid models.

References

[1] B. Aubert *et al.* (BaBar Collaboration), Phys. Rev. Lett. **95**, 142001 (2005).

[2] B. Aubert *et al.* (BaBar Collaboration), arXiv:0808.1543 [hep-ex], (2008).

[3] T. E. Coan *et al.* (CLEO Collaboration), Phys. Rev. Lett. **96**, 162003 (2006).

[4] Q. He *et al.* (CLEO Collaboration), Phys. Rev. D **74**, 091104 (2006).

[5] C. Z. Yuan *et al.* (Belle Collaboration), Phys. Rev. Lett. **99**, 182004 (2007).

[6] B. Aubert *et al.* (BaBar Collaboration), Phys. Rev. Lett. **98**, 212001 (2007).

[7] X. L. Wang *et al.* (Belle Collaboration), Phys. Rev. Lett. **99**, 142002 (2007).

[8] G. J. Ding *et al.*, Phys. Rev. D **77**, 014033 (2008); A. M. Badalian, B. L. G. Bakker, I. V. Danilkin, Phys. Atom. Nucl. **72**, 638 (2009).

[9] M. V. Voloshin, arXiv:hep-ph/0602233 (2006).

[10] S. Dubynskiy, M. B. Voloshin, Phys. Lett. B **666** 344, (2008).

Table 1: The upper limits on the peak cross section for the processes $e^+e^- \to X \to D^0D^{*-}\pi^+$ at $E_{\rm c.m.} = m_X$, $\mathcal{B}_{\rm ee}\times\mathcal{B}(X \to D^0D^{*-}\pi^+)$ and $\mathcal{B}(X \to D^0D^{*-}\pi^+)/\mathcal{B}(X \to \pi^+\pi^- J/\psi(\psi(2S))$ at the 90% C.L., where $X = Y(4260)$, $Y(4350)$, $Y(4660)$, $X(4630)$.

	$Y(4260)$	$Y(4350)$	$Y(4660)$	$X(4630)$
$\sigma(e^+e^- \to X) \times \mathcal{B}(X \to D^0D^{*-}\pi^+)$, [nb]	0.36	0.55	0.25	0.45
$\mathcal{B}_{\rm ee} \times \mathcal{B}(X \to D^0D^{*-}\pi^+)$, [$\times 10^{-6}$]	0.42	0.72	0.37	0.66
$\mathcal{B}(X \to D^0D^{*-}\pi^+)/\mathcal{B}(X \to \pi^+\pi^- J/\psi)$	9			
$\mathcal{B}(X \to D^0D^{*-}\pi^+)/\mathcal{B}(X \to \pi^+\pi^-\psi(2S))$		8	10	

[11] For example: L. Maiani, V. Riquer, F. Piccinini, A. D. Polosa, Phys. Rev. D **72**, 031502 (2005); D. Ebert, R. N. Faustov, V. O. Galkin, Eur. Phys. J. C **58**, 399 (2008).

[12] X. Liu, X.-Q. Zeng, X.-Q. Li Phys.Rev. D **72**, 054023 (2005); G.-J. Ding, Phys. Rev. D **79**, 014001 (2009).

[13] For example: S. L. Zhu, Phys. Lett. B **625**, 212 (2005); F. E. Close, P. R. Page, Phys. Lett. B **628**, 215 (2005); E. Kou, O. Pene, Phys. Lett. B **631**, 164 (2005).

[14] Charge-conjugate modes are included throughout this paper.

[15] G. Pakhlova *et al.* (Belle Collaboration), Phys. Rev. D **77**, 011103 (2008).

[16] G. Pakhlova *et al.* (Belle Collaboration), Phys. Rev. Lett. **98**, 092001 (2007).

[17] G. Pakhlova *et al.* (Belle Collaboration), Phys. Rev. Lett. **100**, 062001 (2008).

[18] G. Pakhlova *et al.* (Belle Collaboration), Phys. Rev. Lett. **101**, 172001 (2008).

[19] G. Pakhlova *et al.* (Belle Collaboration), arXiv:0801.3418 [hep-ex] (2008).

[20] A. Abashian *et al.* (Belle Collaboration), Nucl. Instrum. Meth. A **479**, 117 (2002).

[21] S. Kurokawa and E. Kikutani, Nucl. Instrum. Meth. A **499**, 1 (2003); and other papers included in this volume.

[22] Since only charged final states are measured, our results should be scaled by a factor of two for this comparison.

[23] B. Aubert *et al.* (BaBar Collaboration), Phys. Rev. D **79**, 092001 (2009).

[24] D. Cronin-Hennessy *et al.* (CLEO Collaboration), arXiv:0801.3418 [hep-ex] (2008).

[25] B. Aubert *et al.* (BaBar Collaboration), Phys.Rev. D **76**, 111105 (2007).

[26] S. Dobbs *et al.* (CLEO Collaboration), Phys. Rev. D **76**, 112001 (2007).

[27] M. Ablikim *et al.* (BES Collaboration), Phys. Lett. B **630**, 14 (2005).

[28] C. Amsler *et al.* (Particle Data Group), Phys. Lett. B **667**, 1 (2008).

[29] M. Ablikim *et al.* (BES Collab.), Phys. Lett. B **660**, 315 (2008).

[30] B. Aubert *et al.* (BaBar Collab.), Phys. Rev. D **76**, 092006 (2007).

[31] J. Segovia, D. R. Entem, F. Fernandez, arXiv:0810.2875 [hep-ph](2008); B. Q. Li and K. T. Chao, Phys. Rev. D **79**, 094004 (2009).

[32] For example: S. Anderson *et al.* (CLEO Collaboration), Phys. Rev. Lett. **86**, 2732 (2001); K. Abe *et al.* (Belle Collaboration), Phys. Rev. Lett. **89**, 151802 (2002); K. Abe *et al.* (Belle Collaboration), Phys. Rev. Lett. **88**, 181803 (2002); M. Z. Wang *et al.* (Belle Collaboration), Phys. Rev. Lett. **90**, 201802 (2003); N. Gabyshev *et al.* (Belle Collaboration), Phys. Rev. Lett. **97**, 242001 (2006); J. L. Rosner, Phys. Rev. D **68**, 014004 (2003); Eef van Beveren, X. Liu, R. Coimbra, G. Rupp, Europhys. Lett. **85**, 61002 (2009); Eef van Beveren, G. Rupp, arXiv:0908.0242 [hep-ph](2009).

[33] Z. Q. Liu, X. S. Qin and C. Z. Yuan, Phys. Rev. D **78**, 014032 (2008).